Investigation of a Modified Circular Nozzle for Cold Spray Applications

Amit Kumar Sharma, Ashish Vashishtha, Dean Callaghan
Department of Aerospace and Mechanical Engineering, South East Technological University, Carlow, Ireland,
The Centre of Research and Enterprise in Engineering (engCORE), South East Technological University, Carlow, Ireland

Srinivasan Rao Bakshi, M. Kamaraj
Department of Metallurgical and Material Engineering, Indian Institute of Technology Madras, Chennai, India

Ramesh Raghavendra
SEAM Research Centre, School of Engineering, South East Technological University, Waterford, Ireland

Abstract

The current work numerically evaluates the efficacy of a co-flowing nozzle for cold spray applications with the aim to mitigate nozzle clogging by reducing the length of its divergent section. The high-pressure nitrogen flow through convergent-divergent axis-symmetric nozzles was simulated and the particle acceleration is modelled using a 2-way Lagrangian technique which is validated using experimental results. An annular co-flow nozzle with a circular central nozzle has been modelled for nitrogen gas. Reduction of nozzle divergent length from 189 mm to 99 mm showed an approximate 2.2% drop in particle velocity at high pressure operation while no variation at lower pressure operation was observed. Co-flow was introduced to the reduced nozzle length to compensate for particle velocity loss at higher operating conditions and it was found that co-flow facilitates momentum preservation for primary flow resulting in increased particle speed for a longer axial distance after the nozzle exit. The reduced divergent section nozzle, when combined with co-flow, is comparable to the original length nozzle.

Introduction

Cold gas dynamic spray (cold spray) has emerged to be the most attractive non-thermal metal deposition process that has garnered significant interest from researchers and industry due to its potential in the coating and additive manufacturing fields [1]. During the cold spray process, particles are accelerated at high pressure with a preheated supersonic gas stream above the critical velocity, but below the erosion velocity, to achieve the bonding [2]. The performance of a cold spray system can be assessed by deposition quality & efficiency and powder acceleration. The three main parameters affecting the performance are input power (gas stagnation pressure and temperature at nozzle upstream), powder & substrate material properties and the nozzle design. The two most commonly utilized carrier gases are nitrogen and helium. Higher consumption of the carrier gases during operation and clogging phenomenon occurring in the divergent section of nozzle are the two main bottlenecks to be resolved for long continuous operations of a cold spray system. Clogging generally occurs when fast moving particles bond to the nozzle's inner surface instead of continuing downstream towards the substrate. The particles gradually build up and obstruct the nozzle passage inhibiting deposition onto the substrate. Additionally, particle layers adhered on the inside surface of nozzle reduces the working cross-sectional area. This lowers the flow velocity and therefore lowers particle velocity, compromising the particles' capacity to reach their critical velocity at the substrate. Materials known for their propensity to clog include aluminum, copper, nickel, stainless steel, inconel, and titanium [3-7]. Cold spray nozzles are often manufactured from materials such as tool steel, alloys, metal carbides and cermets, making it uneconomical to change clogged nozzles frequently owing to the high costs involved [8-10].

Although it is possible to clean nozzles and restore them to their original specifications, this necessitates cumbersome machining processes and additional expense. Spraying a mixture of powders that are prone to clogging and ceramic particles can reduce nozzle clogging [11], but this brings a risk of impinging unwanted material on to the substrate. The two primary factors that contribute to nozzle clogging are the high temperature nozzle wall and particle dispersion as highlighted by Wang et al. [12] which is consistent with the findings of other researchers. It has been seen that the clogged region of the nozzle is typically found towards the last portion of the divergent section of nozzle. Reducing the divergent length of nozzle up to a significant length without compromising the particles exit velocity could potentially eradicate the portions which were frequently prone to clogging during long continuous cold spray operation. Even though the supersonic nozzle is central to a cold spray systems performance, very few studies have been carried out on nozzle designs that enhance deposition efficiency and build quality [13]. In this study a volume of high-speed fluid encircling the primary flow is introduced as a coaxial co-flow nozzle with a view to shortening the divergent section length. Co-axial nozzles have been experimentally studied previously in an open jet facility using sonic co-flow combined with supersonic primary flow [14,15]. It was observed that under all operating conditions, the sonic co-flow around the supersonic jet not only elongated the supersonic core by increasing the number of shock-cells, but also retained momentum in the jet's decay zone. Particle acceleration may increase in the elongated supersonic core length to longer distances. The higher particle acceleration after the nozzle exit can make it possible to shorten the divergent section length, which in turn can reduce clogging and allow for longer periods of continuous system operation. Future coaxial

system operation using various gases can also cut down on the need for a primary particle accelerating carrier gas with the outer gas conserving momentum. In addition, co-flow can also have the added advantage of assisting nozzle wall cooling which in turn could contribute to a reduction in nozzle clogging. Significant advances in computational fluid dynamics (CFD) [16-17] research of cold spray processes enables the performance of the novel nozzle to be evaluated in conjunction with experimentally obtained results. The primary aims of this study are to, 1) find the minimum acceptable divergent length nozzle without performance degradation and 2) improve particle acceleration in a reduced size nozzle with co-flow.

Design and Modelling Method

All the numerical simulations carried out in this study are performed using ANSYS Fluent 2021 R1 with gas and particle simulations carried out using a two-dimensional axis-symmetric computational domain.

Geometry and Computational Domain

The original nozzle has a divergent length (DL) of 189 mm. The exit to throat area ratio and convergent section were kept constant for all nozzle designs while the divergent length was varied 15D to 42D, where D is nozzle exit diameter. The corresponding values of all four designs (DL 189, DL 109, DL 99 & DL 69) with varying divergent length are summarized in Table 1.

Table 1 Simulated Cases (NCF- Without Co-Flow, CF- With Co-Flow, Gas: Nitrogen)

Cases	With/ With-out co-flow	Operating Condition	Material	Particle Size
DL69	NCF	6 MPa & 1273 K	Inconel 718	22 µm, 35 µm
		3 MPa & 623 K	Titanium	
DL99	CF (3 MPa & 300 K) & NCF	6 MPa & 1273 K	Inconel 718	22 µm, 35 µm & (15-35 µm)
		3 MPa & 623 K	Titanium	
DL109	NCF	6 MPa & 1273 K	Inconel 718	22 µm
DL189	NCF	6 MPa & 1273 K	Inconel 718	22 µm, 35 µm & (15-35 µm)
			Titanium	

As illustrated in Fig. 1, a co-flowing annular straight channel is coupled to the divergent portion for the nozzle, allowing the central jet to expand into the sonic annular flow. A straight chamber is attached in the beginning of the convergent section of the nozzle to stabilize the gas flow. The computational domain comprises of a stagnation chamber, a particle discharge tube, the nozzle along with the co-flow region and an extended expansion region. A two-dimensional axis-symmetric model was utilized in the analysis with quadrilateral elements which allows a considerable reduction in computational time. The structured mesh was constructed to complement the respective flow phenomena and tested to provide a mesh-independent solution. The mesh was refined at the near-wall region to capture the boundary layer flow. The throat and exit region of nozzle was refined adequately to visualize flow gradient and capture the shock patterns. Special attention was given to the exit refinement to ensure that there is no change in solution of flow pattern.

Boundary Conditions

The boundary conditions at the nozzle inlet (pressure inlet) were set to 3 MPa and 623 K for titanium particles and 6 MPa and 1273 K for inconel 718 in all of simulations, while atmospheric static pressure was set at the outlet zone. At the co-flow nozzle (pressure inlet) 3 MPa and 300 K were applied in to understand the influence on particle acceleration and enhancement of the primary flow core length. The stagnation chamber has negligible velocity thus the total and static temperature and pressure are equal. An extended domain was created at the exit of the nozzle with the aim of analyzing the particle's velocity profile. For the without co-flow simulation case, the co-flow inlet was assigned a wall boundary condition. The titanium powder particle was 45 µm in size and a mass flow rate of 16 g/min was chosen for all low-pressure particle injection analysis. For Inconel, the particles of 22 µm and 35 µm and a variation of 15-35 µm were injected from the nozzle inlet at 60 g/min.

Simulation Set-Up

The nozzle configurations in Table 1 were simulated with a two-dimensional axisymmetric solver. To account for compressibility effects, the ideal gas law was used for density calculations and nitrogen was used as the process gas.

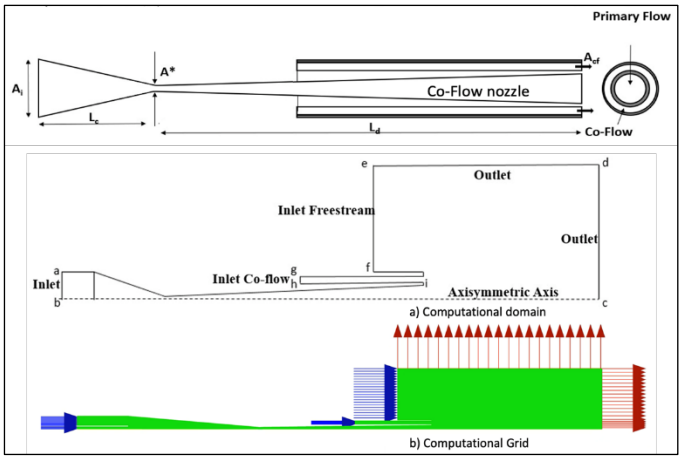

Figure 1 Schematic diagram of nozzle (top), (a) computational domain & (b)computational grid

An implicit density-based solver was used under steady state conditions as it responds favorably to compressible flows in the supersonic region. In highly compressible flow, the viscosity of the gas tends to change with temperature, thus the 3-coefficient Sutherland law is utilized as its widely recommended for supersonic gas flows. The Advection Upstream Splitting Method (AUSM) scheme was employed as the flux type along with the Green-Gauss node based gradient method for discretization. Simulation of flow fields were solved with second-order accuracy until the necessary number of iterations to reach an acceptable level of convergence were achieved. As the flow field lacks regions of flow separation or re-circulation,

the 2-equation standard k-ε model of turbulence was found adequate for this study. High order term relaxation (HOTR) and convergence acceleration for stretched meshes (CASM) were enabled to accelerate convergence in the Density based solver (DBS-implicit) along with solution steering [18]. The FMG initialization method was used to get an initial solution for the solver to initiate the simulation and reduce the computational time. Particle injection into the nozzle inlet was carried out using a discrete phase modelling algorithm. A two-way Lagrangian approach was utilized to simulate particle acceleration, as it is more effective for obtaining higher quality results. Furthermore, the high-Mach number drag law was used to include the effect of compressibility. The stochastic-tracking type model discrete random walk (DRW) method was used to account for particle dispersion due to turbulence effects. By using this, the generation of a fluctuating velocity is realized by a Gaussian distribution function. [18]

Grid Independence and Model Validation

Three different mesh sizes of grids fine (0.075 mm), medium (0.1 mm) and coarse (0.125 mm) were used to simulate the central nozzle without co-flow.

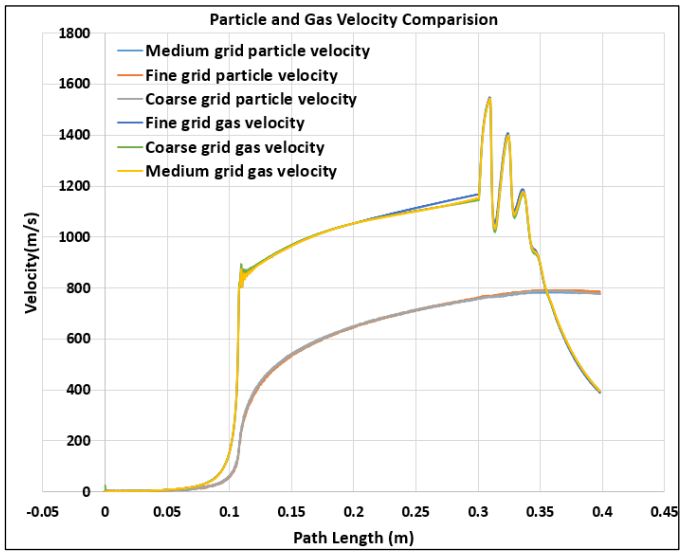

Figure 2 Grid Independence test for different grid sizes

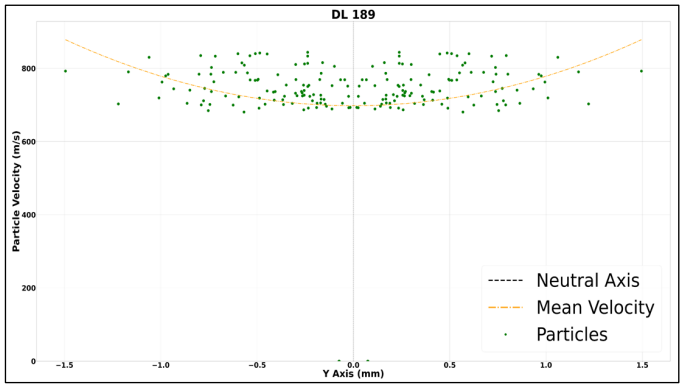

Figure 3 Particle velocity distribution with lateral axis

Particles were injected at the nozzle inlet. Gas and particle velocities have been plotted against path length as shown in Fig. 2. There is no significant difference in particle acceleration among the three grids and the medium grid was selected for further computation to reduce computation time.

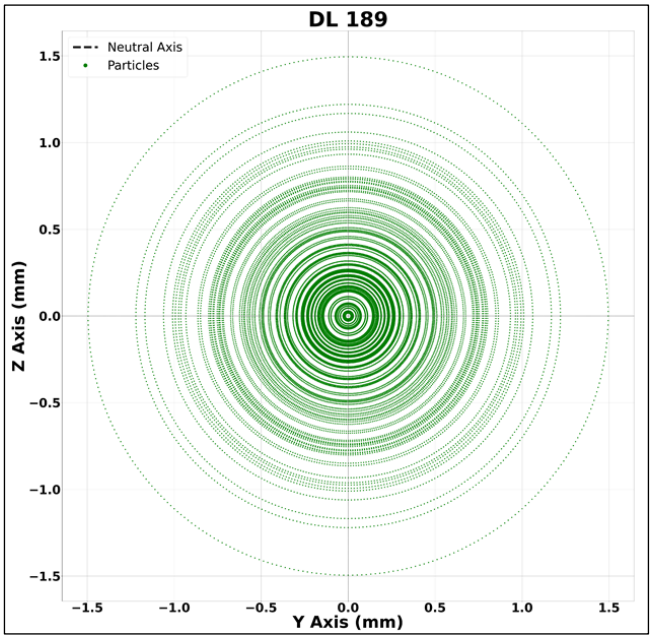

Figure 4 Indicative particle position at 25mm standoff distance from the nozzle exit

Furthermore, the simulation for inconel particles of sizes ranging 15 µm to 35 µm were carried out and compared with the experimental data at a 25 mm stand-off distance as shown in Fig. 3 and Fig. 4. It can be seen that the simulation results are comparable to the experimental results where particle speeds were found to be well matched (private communication IIT Madras) [19] and thus validating the numerical model.

Results and Discussion

Generally cold spray system nozzles have a circular cross-section, with longer divergent length and an outlet diameter less than 10 mm. The longer divergence section might cause the nozzle wall's boundary layer to engage with the center-line flow resulting in increased friction losses. However, when compared to isentropic design values, friction losses can raise the exit temperature of a gas. Furthermore, the long length of the nozzle necessitates repeated cleaning during continuous operation as they are susceptible to clogging. This study investigates the effect of a reduced divergent length on particle acceleration in order to understand whether a smaller divergent length nozzle could be as effective as the original nozzle. The study also investigates the effect of using a co-flow nozzle over the reduced divergent length to compensate for any loss in particle momentum due to reduction in the divergent length. The sections that follow will analyze the results of the axis-symmetric numerical simulations for four different divergent length nozzles on particle acceleration. In addition, shorter nozzles using co-flow are compared with the original nozzle while maintaining the same exit and throat cross-section area, to understand the effectiveness of the co-flow.

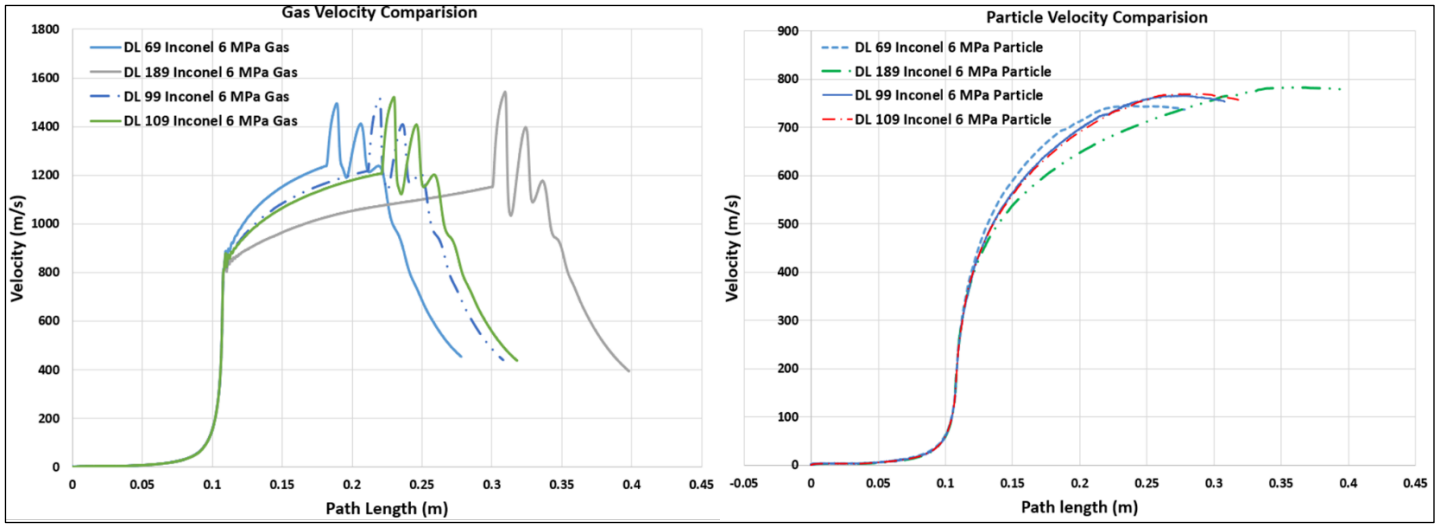

Figure 5 Axial gas velocity and particle velocity DL 69, 99, 109 & 189 at 6 MPa 1273K Inconel for 22 µm particle size

Reduction of the Divergent Length

Figure 5 depicts the gas phase velocity variation and particle velocity while Fig. 6 shows the corresponding contour plots for the gas velocity magnitude along the axial distances for the different divergent nozzles at 6 MPa gas pressure and 1273 K gas temperature. The gas velocity profiles follow the same trend in the convergent section of the nozzle and the supersonic jet profile, the number of shock cells at outlet also looks similar. It can be seen that as the length of the nozzles become shorter and the gas exit velocities increase due to a reduced boundary layer effect and friction losses. However, particle velocities for smaller divergent section nozzles can reach lower maximum speeds than the longer divergent section nozzles. It is evident that longer nozzles can allow a longer residence time for particles to remain in high-speed flow to impart higher speed, but shorter nozzles cannot. But up to a certain reduction in divergent length the particle speed doesn't drop significantly or in some cases remains unaltered. In this study three different divergent length nozzles, DL 109, DL 99, and DL 69 were simulated along with the original length DL 189 nozzle to find the critical length at which the performance of the nozzle starts dropping. The particle speeds up to the DL 119 nozzle were very close to the performance to that the DL 189 nozzle and some significant difference was seen from DL 109 onwards. A 22 µm particle size was selected for all simulations. The particle maximum velocity reduces from 783 m/s in DL 189 to 769 m/s, 765 m/s and 744 m/s in DL 109, DL 99, DL 69 respectively.

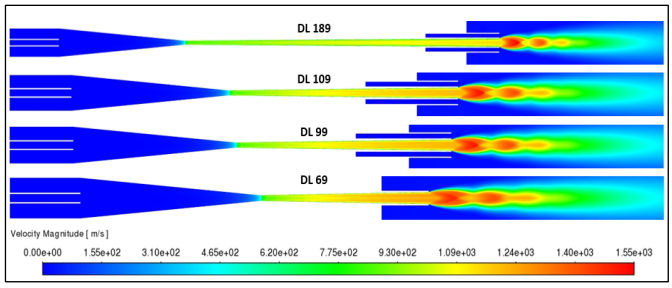

Figure 6 Gas velocity contours for DL 69, 99, 109 & 189 at 6 MPa 1273K Inconel for 22 µm particle size

Between DL189 and DL 69 there is approximately a 6.0 % drop in the velocity while with DL 109 & DL99 there is a 1.7 % and 2.2 % drop. In cold spray the critical velocity is defined by the velocity needed by the slowest moving particle to bond with the substrate and the slowest particle tend to be the particles of larger diameter. Thus, these large diameter particles dictate the optimum parameters of gas temperature and pressure for the process. Inconel 718 powder has a particle size distribution between 15-35 µm with a mean diameter as 22 µm. Therefore, additional simulations were carried out for the shorter divergent nozzle using a 35 µm particle size to observe the effect it has on the particle velocities.

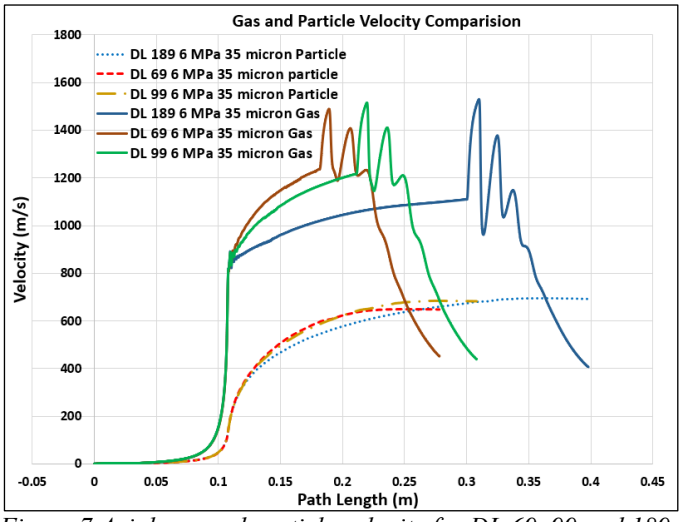

Figure 7 Axial gas and particle velocity for DL 69, 99 and 189 at 6 MPa 1273 K for 35 µm particle size

Figure 7 shows the gas velocities and particle velocities for an inconel particle of size 35µm.The gas velocity profile behaves the same way as mentioned before being the highest for DL 69 and lowest for DL 189 nozzle. DL 99 gas velocity at the outlet shows minimal difference when compared to the DL 69 indicating that the losses are not that significant in this range for

the divergent section of the nozzle. Comparing the particle velocities, the 35 µm particle attained 695 m/s in DL 189, 685 m/s in DL 99 and 650 m/s in DL 69 case. This indicates that DL99 sustained a 1.4% drop in velocity while DL 69 had a 6.5% drop in comparison to the original length nozzle. Comparing the particle velocity results from both 22 µm and 35 µm simulation case, DL 99 would be a better choice for reducing the divergent length without large compromise in performance of the nozzle with just a variation of nearly 2% with DL189.

When a nozzle is designed for a cold spray system the nozzle has to accommodate different material types across a range of pressure and temperatures. It is required to validate the reduced divergent length nozzle at lower pressure and temperature conditions for use over a wide range of particle deposition.

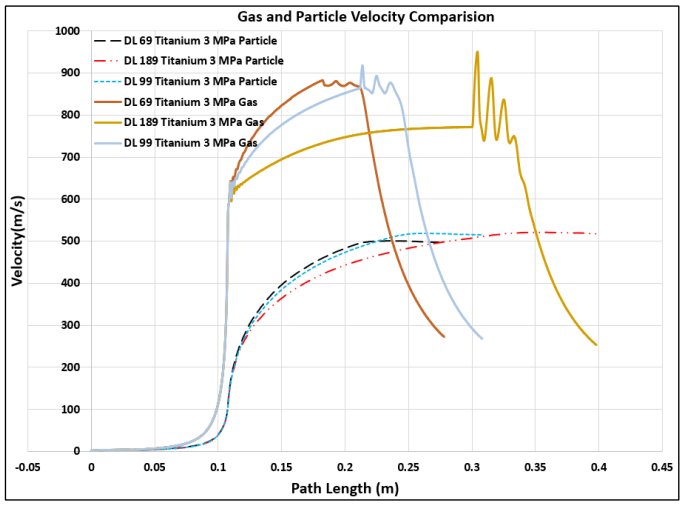

Figure 8 Axial gas velocity and particle velocity for DL 69, 99 & 189 at 3 MPa 623 K for 45 µm Titanium particles

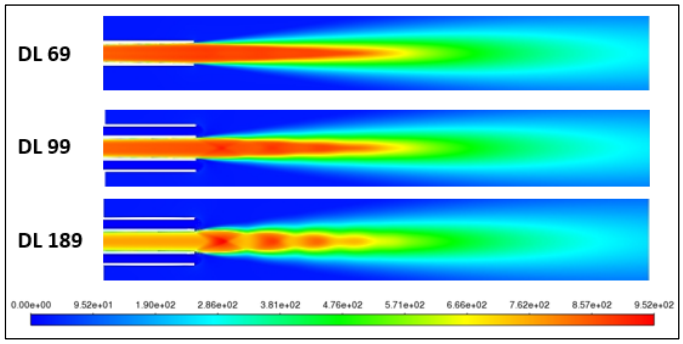

Figure 9 Gas velocity contours for DL 69, 99 & 189 at 3 MPa 623 K for 45 µm titanium particles

Additional simulations were carried out at 3 MPa 623K for titanium particles of size 45 µm for the DL189, 99 and 69 nozzles. Figure 8 shows the gas and particle velocity profiles and Fig. 9 shows the gas velocity magnitude contours. Observing the gas profile and its velocity contours at outlet for DL 69 and DL 99, it can be seen that the shocks are diminished with respect to DL 189 and there is a smooth gas velocity curve. Comparing the particle velocities, it can be seen that the titanium particles reached a maximum velocity of 521m/s in the case of the DL 189 and sustained a 4% drop in velocity compared to 501m/s for the DL69. It's notable that DL 99 showed minimal decrease in particle velocity compared to that of the original nozzle.

This would suggest that the performance of the reduced divergent nozzle is more effective at lower pressure and temperatures. This could be due to reduced fictional losses in the gas stream at lower gas speeds in the nozzle. It can be concluded that for lower pressure operation the divergent section can be reduced up to a 99 mm divergent length without experiencing significant performance loss.

The Effect of Co-Flow

In light of the above discussion about the performance of nozzles at high and low-pressure for two different material types and different particle sizes, it can be concluded that the DL 99 case offers the shortest divergent length nozzle without sustaining significant losses in particle velocity. At a pressure of 6 MPa the particle velocity drop was 2.2 % for DL 99. To compensate for this loss the addition of co-flow was introduced to the nozzle. Figure 10 shows the particle velocity comparison between DL 99 with coflow and DL 189 cases for particle size of 22 µm and 35 µm.

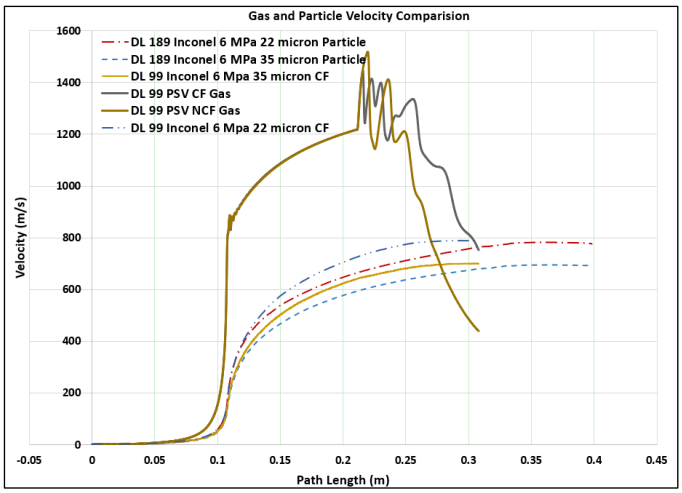

Figure 10 Axial particle velocity comparison between DL 99 CF & DL 189 for 22 and 35 µm particle size and gas velocity comparison between DL 99 CF and DL99 NCF for particle size distribution 15-35 µm

For a particle size of 35 µm DL 99 CF a particle velocity of 700 m/s was found compared to 695 m/s of DL 189. Similarly, for the 22 µm particle size, DL 99 CF reached a velocity of 789 m/s compared to 783 m/s of DL 189. In the co-flow case once, maximum particle velocity is reached, the particles carry on a constant velocity for a larger standoff distance compared to no co-flow cases where the velocity drop is evident after particle reaches maximum velocity. The co-flow nozzle has been found to preserve momentum of gas in the central jet flow. Using co-flow, the flow-field significantly changes as the supersonic core length increases to longer axial distances as the high-speed annular flow reduces the mixing of the supersonic core with surrounding nozzle and prolongs the velocity decay. This indicates that the use of co-flow in DL 99 provides enhanced performance compared to the original nozzle.

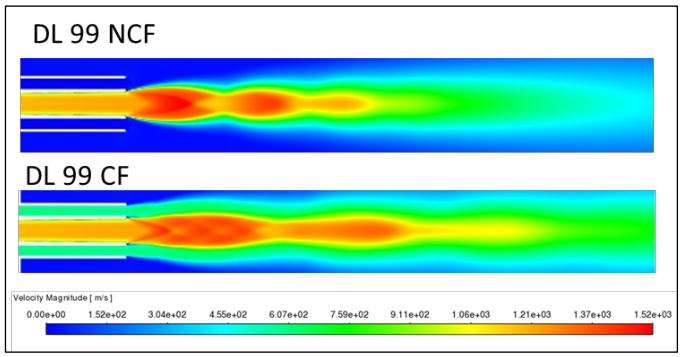

Figure 11 Gas velocity contours comparison between DL 99 CF and DL99 NCF for particle size distribution 15-35 µm

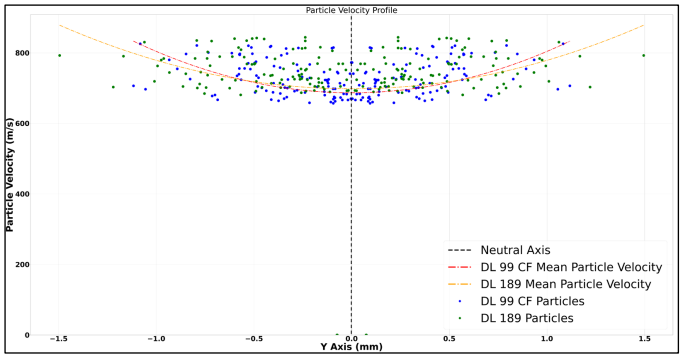

Figure 12 Particle velocity distribution of DL 99 CF and DL189 case with lateral axis

Simulations were carried out for the DL 99 CF and the NCF conditions with a particle size distribution of between15-35 µm. Figure 10 shows the gas velocity profiles & Fig. 11 the gas velocity magnitude contours under the same conditions. The supersonic core length can be defined as the point of the last shock-cell from the nozzle exit. The gas velocity decays rapidly for no co-flow, due to the increased mixing caused by high entrainment of mass from the surroundings while the co-flow case maintains the velocity for longer distances. From the contour plots it is evident that the core length has increased for the co-flow case helping the particle maintain momentum for longer lengths.

Figure 12 shows the particle speed distribution for both DL 99 CF and DL189 with particle sizes ranging between 15µm and 35µm and Fig.13 shows the mean velocity comparison. The mean velocity plot shows that the particle continues to accelerate after exit for a greater standoff distance and ultimately reaches a higher mean velocity than the original DL 189 nozzle. Looking at the particle position in Fig. 14 and the velocity distribution in Fig.12, it can be seen that particle dispersion is less in the DL 99 CF when compared to DL 189 with particle density closer to the neutral axis. Comparing this with the DL 189 simulation and the experimental results, it can be said that the DL 99 with co-flow seems to be an optimal choice providing enhanced performance over the DL189 with its deposition capability over a larger distance, higher mean velocity, less prone to frictional losses and possibly reducing clogging.

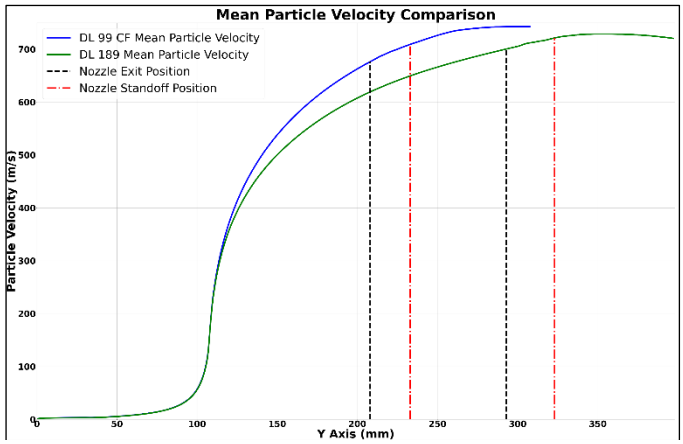

Figure 13 Mean particle velocity comparison for DL 99 CF and DL 189 case

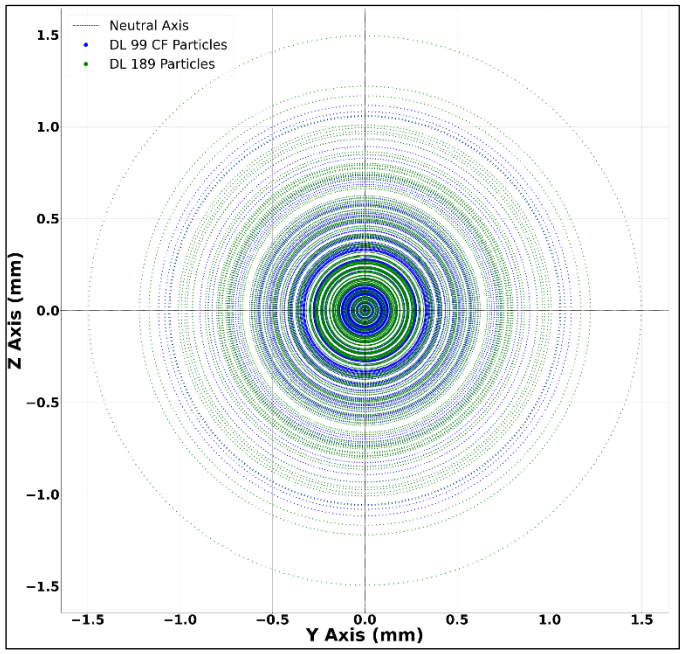

Figure 14 Indicative particle position for DL99 CF and DL 189 at 25mm standoff distance from the nozzle exit

Conclusion

In this analysis, the effect of a reduction in the divergent section of a cold spray nozzle along with the addition of an outer co-flow nozzle was studied. The key findings to date are:

1. Reducing the divergent section length increases the exit gas velocity from the nozzle while also leading to a reduction in the residence time for particles in a high-speed stream, which reduces the particle's maximum attainable velocity. However up to a certain reduced divergent length there is reduced variation in the particle velocity compared to the original nozzle.
2. Based on supersonic core-length elongation, the DL 99 CF nozzle with co-flow has comparable performance with the DL 189 NCF nozzle without co-flow for gas velocity and particle acceleration. The introduction of an outer co-flow in the reduced divergent section nozzle improves the performance at

all the lengths for supersonic core elongation as well as enhancing particle acceleration.

3. It is expected that the reduced divergent length will facilitate the reduction of clogging and lead to enhanced continuous operational time of cold spray equipment. This will be explored further in a follow-on study of this current research.

References

1. R.N. Raoelison, *et al.,* "Cold gas dynamic spray additive manufacturing today: Deposit possibilities, technological solutions and viable applications," *Materials & Design*, Vol. 133 (2017), p 266-287. https://doi.org/10.1016/j.matdes.2017.07.067.
2. M. Kamaraj, *et al.,* "Cold Spray Coating Diagram: Bonding Properties and Construction Methodology," *J Therm Spray Tech* **28** (2019), p 756–768. https://doi.org/10.1007/s11666-019-00853-5
3. D. Poirier, *et al.,* "Powder Development and Qualification for High-Performance Cold Spray Copper Coatings on Steel Substrates," *J Therm Spray Tech* **28** (2019), p 444–459. https://doi.org/10.1007/s11666-019-00833-9
4. P. Liebersbach, *et al., "*CFD Simulations of Feeder Tube Pressure Oscillations and Prediction of Clogging in Cold Spray Nozzles," *J Therm Spray Tech* **29** (2020), p 400–412. https://doi.org/10.1007/s11666-020-00992-0
5. A. Sova, *et al.,* "Cold spray deposition of 316L stainless steel coatings on aluminium surface with following laser post-treatment," *Surface and Coatings Technology,* Volume 235 (2013), p 283-289. https://doi.org/10.1016/j.surfcoat.2013.07.052.
6. V.K. Champagne Jr., *et al.,* "Magnesium Repair by Cold Spray." *Plating and Surface Finishing* 95 (2008), p 19-28.
7. W. Wong, *et al.* "Cold Spray Forming of Inconel 718," *J Therm Spray Tech* **22** (2013), p 413–421. https://doi.org/10.1007/s11666-012-9827-1
8. WY. Li, *et al.,* "An Investigation on Temperature Distribution Within the Substrate and Nozzle Wall in Cold Spraying by Numerical and Experimental Methods," *J Therm Spray Tech* **21** (2012), p 41–48. https://doi.org/10.1007/s11666-011-9685-2
9. Ozan C. Ozdemir, *et al.,* "Gas dynamics of cold spray & control of deposition," *South Dakota School of Mines & Technology*, 01/31/2017.
10. T. Suhonen, *et al.,* "Residual stress development in cold sprayed Al, Cu and Ti coatings," *Acta Materialia*, Volume 61, Issue 17 (2013), p 6329-6337. https://doi.org/10.1016/j.actamat.2013.06.033
11. H. Koivuluoto, *et al.,* "Effect of Ceramic Particles on Properties of Cold-Sprayed Ni-20Cr+Al_2O_3 Coatings," *J Therm Spray Tech* **18** (2009), p 555–562. https://doi.org/10.1007/s11666-009-9345-y
12. X. Wang, *et al.,* "Investigation on the Clogging Behavior and Additional Wall Cooling for the Axial-Injection Cold Spray Nozzle," *J Therm Spray Tech* **24** (2015), p 696–701. https://doi.org/10.1007/s11666-015-0227-1
13. R.N. Raoelison, *et al.,* "Cold gas dynamic spray technology: A comprehensive review of processing conditions for various technological developments till to date," *Additive Manufacturing*, Volume 19 (2018), p134-159. https://doi.org/10.1016/j.addma.2017.07.001
14. H. Sharma, *et al.,* "Characteristics of sonic and supersonic co-flow jets," *Proceedings of 2nd International Conference on Recent Advances in Experimental Fluid Mechanics* (RAEFM), March 2008.
15. H. Sharma, *et al.,* "Experimental study of overexpanded co-flowing jets," *The Aeronautical Journal*, 112(1135), p 537-546. https://doi.org/10.1017/S0001924000002499
16. M. Meyer, e*t al.,* An analysis of the particulate flow in cold spray nozzles, *Mech. Sci.,* 6, (2015), p 127–136. https://doi.org/10.5194/ms-6-127-2015
17. Xinkun Suo, *et al.,* "Strong effect of carrier gas species on particle velocity during cold spray processes," *Surface and Coatings Technology*, 268:90–93, 2015. 6th Rencontres Internationales de la Projection Thermique.
18. A.K. Sharma, et al., "Particle Acceleration Through Coaxial Co-Flow Nozzles for Cold Spray Applications." *Proceedings of the ITSC2022. Thermal Spray 2022*: *Proceedings from the International Thermal Spray Conference*, Vienna, Austria. May 4–6 (2022), p 676-682.ASM. https://doi.org/10.31399/asm.cp.itsc2022p0676
19. "Private Communication", with Department of Metallurgical and Material Engineering, Indian Institute of Technology Madras, India